batteries

MDPI

Article

Numerical Study on the Fire Characteristics and the Water Mist Suppression Performance for Lithium-Ion Battery Boxes on Storage Shelves

Qinwei Zhang [1,*], Lilin Yin [2], Han Zhang [1], Wenhao Hua [1], Zelin Zhang [1] and Bin Zheng [1,*]

[1] Department of Fire Protection Engineering, China Fire and Rescue Institute, Beijing 102202, China
[2] Analytical and Testing Center, Northeastern University, Shenyang 110819, China
* Correspondence: zhangqw@cfri.edu.cn (Q.Z.); zhengbin@cfri.edu.cn (B.Z.)

Abstract

Lithium-ion batteries (LIBs) have been widely used in electric vehicles and energy storage systems. Due to their high energy density and complex structural components, thermal runaway of LIBs can lead to severe fire and explosion hazards. Densely arranged LIBs in storage scenarios are highly susceptible to fire propagation, posing challenges to fire safety. In this paper, full-scale LIB box storage shelf models were established using an FDS (Fire Dynamics Simulator) based on the actual shelf configurations. The fire propagation characteristics following thermal runaway were discussed considering common shelf types, the horizontal spacing of adjacent LIB boxes and the longitudinal shelf spacing. Furthermore, the suppression performance of a water mist system was analyzed under varying droplet sizes and spray cone angles. The simulation results indicated that, under the investigated conditions and periods, selecting the shelf with side panels and perforated bottom layers, increasing the horizontal spacing of LIB boxes to 0.8 m and the longitudinal shelf spacing to 1.5 m could effectively reduce the range and combustion intensity of fire propagation. In addition, the water mist system exhibited the most favorable cooling and thermal mitigation performance at a droplet size of 50 μm and a spray cone angle of 75°.

Keywords: LIB box; storage shelf; water mist; fire propagation; thermal mitigation; FDS simulations

1. Introduction

LIBs are widely applied in electric vehicles and energy storage stations in China, driven by China's carbon peaking and carbon neutrality goals. For example, in 2025, new energy vehicle production in Guangdong Province, China, reached 1.0161 million units. The cumulative installed capacity of new energy storage in China reached 144.7 GW by the end of 2025. LIBs exhibit high energy density, long cycle life, low memory effect, and environmental friendliness advantages [1–4]. Various initiating factors, including electrical abuse, mechanical abuse, thermal abuse and inherent manufacturing defects, can easily trigger thermal runaway in LIBs, accompanied by substantial energy release [5–7]. In particular, large quantities of high-state-of-charge (SOC) and high-capacity battery cells, packs, or modules are densely stored during LIB formation, aging, and capacity grading and within the finished battery storage workshop [8]. Once LIBs thermal runaway occurs, the fire spreads rapidly, accompanied by a sharp increase in temperature and the release of large amounts of toxic gases. These hazardous conditions pose substantial challenges in firefighting and rescue operations [9,10]. For instance, in 2024, an LIB fire broke out

Check for updates

Academic Editor: Roberto Bubbico

Received: 21 September 2026
Revised: 10 October 2026
Accepted: 14 October 2026
Published: 16 October 2026

Copyright: © 2026 by the authors. Licensee MDPI, Basel, Switzerland. This article is an open access article distributed under the terms and conditions of the Creative Commons Attribution (CC BY) license.

in South Korea, involving successive battery explosions and lasting for more than 5 h, ultimately resulting in 23 fatalities and 8 injuries. In China, various standards such as the Chinese national standard Code for Fire Protection Design of Buildings (GB 50016) [11] and the Safety Code for Storage and Use of LIBs in Production and Business Units (Shenzhen City Local Standard) [12] provide valuable guidance for the fire protection design and safety management of LIB storage. However, further detailed studies are required to investigate the effects of key factors, such as battery type, battery capacity, shelf type, shelf spacing, and fire facility parameters, on fire propagation dynamics and fire suppression strategies. In fact, full-scale fire experiments in LIB storage scenarios are usually challenging to conduct due to high safety risks, expensive experimental costs, practical implementation difficulties, and instability in data acquisition and monitoring.

In recent years, extensive numerical studies have been conducted to investigate the fire spreading law of LIB storage. For example, Huang et al. [13] performed FDS simulations by varying the cathode materials and ambient temperatures to study 18650-type battery flame behavior, especially in the thermal runaway row-to-row propagation speed. Xie et al. [14] employed FDS to investigate the effects of LIB SOC and shelf spacing on thermal runaway propagation. It was found that lower SOC, appropriate shelf spacing and fast-response automatic sprinkler systems could effectively mitigate fire propagation. Cui et al. [15] developed a battery pack model based on a real warehouse setting. The simulation results indicated that following thermal runaway in the initial battery pack, flames preferentially spread upward and impacted the upper battery pack after 19 s, whereas horizontal flame propagation was strongly correlated with battery pack spacing. Using multi-physics simulations, Mishra et al. [16] demonstrated the existence of a critical threshold value for the pallet gap during the large-scale storage and transportation of LIBs beyond which fire propagation ceased to occur. Wang et al. [17] explored the effects of ambient pressure on battery combustion through simulation analysis. The results revealed that battery combustion at high altitudes accelerated the formation of high-temperature regions and increased fire propagation rates, ultimately prolonging the fire duration. Lou et al. [18] established a 1:1 simulation geometry model of a container LIB energy storage cabin and studied the optimal parameters of a water mist sprinkler system, including spray intensity, fog cone angle, nozzle velocity, and water mist size, to optimize the safety design and fire protection.

In this paper, we performed a series of LIB fire simulation experiments based on the actual configurations of LIB storage shelves containing lithium manganese oxide (LMO) batteries. The effects of storage shelf type, horizontal spacing between LIBs, and longitudinal spacing between shelves on LIB fire spread behavior were investigated, with particular emphasis on the heat release rate (HRR), the temperature variations above the ignition sources, the temperature variations at the top of the shelf, and heat transfer between adjacent LIB boxes. Furthermore, the water mist system was adopted as the initial fire protection measure against the LIB fire. The key factors such as the water mist droplet sizes and spray cone angles were discussed to identify the most effective parameter combination under the investigated situations, thereby gaining a critical time window for emergency response. For LIB storage scenarios, our study provides a theoretical reference for further optimizing shelf layouts and safety design and enhancing fire safety management.

2. Materials and Methods

2.1. LIB Storage Shelf Model Design

As shown in Figure 1, LIB boxes were arranged with a specified horizontal spacing within the shelf compartment. Each LIB box consisted of 3000 18650 LMO batteries, each with a nominal capacity of 1700 mAh, a nominal voltage of 3.7 V, and an initial SOC of

100%, corresponding to a total nominal energy of 18.87 kWh per LIB box. The LIB box had dimensions of 0.8 m × 0.8 m × 0.4 m. The shelf measured 6.2 m × 1 m × 5 m, with 6 layers and a vertical spacing of 0.8 m between adjacent layers. The shelf structure, composed of the side baffles and the bottom layers, was modeled using cold-rolled steel with a density of 7850 kg/m^3, a specific heat capacity of 460 J/(kg·K), and a thermal conductivity of 45.80 W/(m·K). The surface emissivity was specified as 0.95. Each side baffle had overall dimensions of 0.2 m × 1.0 m × 5.0 m. The bottom layer had overall dimensions of 1.4 m × 1.0 m × 0.2 m. Thermocouples were positioned 0.1 m above each LIB box to monitor temperature variations across the shelf during fire propagation. Water mist devices were installed 0.15 m above each LIB box to suppress fire propagation. In the practical storage, the shelf support layers beneath the LIB boxes were commonly constructed from hollow metal wire mesh.

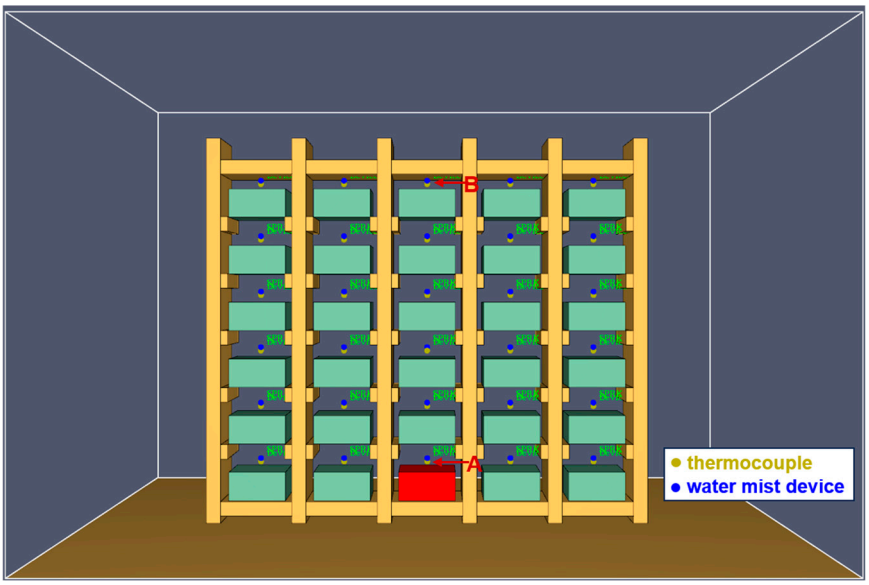


Figure 1. Schematic diagram of LIB storage shelf model (Red box represented the ignition source).

To simplify the model, the support layers were represented as perforated metal surfaces to allow gas flow through the vertical direction between adjacent layers, thereby approximating the actual condition. Except for the bottommost layer, rectangular openings measuring 0.8 m × 1 m ×0.2 m were introduced into each bottom layer with a 57% open-area ratio. Importantly, the red box in Figure 1 was designated as the ignition source, representing the first LIB box to undergo thermal runaway. The fire source area of the red box was 1.92 m^2. Temperature monitoring Point "A" was located above the ignition source, while temperature monitoring Point "B" was located at the top of the shelf.

2.2. Numerical Simulation Methods and Parameter Settings

FDS software was employed to simulate horizontal and vertical fire propagation processes in different LIB fire conditions and to evaluate the fire suppression effectiveness of the water mist system under different parameter settings. All simulations were performed using FDS 6.9.1. The computational domain had dimensions of 9.7 m × 8.0 m × 6.4 m, which was discretized into a large number of computational cells. The four lateral boundaries and the upper boundary were specified as open pressure boundaries, whereas the floor and the shelf were treated as solid boundaries. The arrangement allowed gases to leave the computational domain and ambient air to enter through the open boundaries. The initial ambient temperature and pressure were set to 20 °C and 101,325 Pa, respectively. The governing equations were solved based on the mass, momentum, and energy conservation

principles to obtain the transient fire flow field, temperature, and species concentration [19]. The Large Eddy Simulation (LES) method was adopted to resolve turbulent flow [20,21]. The simulation results were visualized via Smokeview to illustrate fire spreading processes, temperature distributions, and water mist spray effectiveness.

LIB was composed of a positive electrode, negative electrode, separators, electrolytes, and other complex components. Owing to numerous and complex combustion reactions, it was difficult to directly define reaction parameters or select a specific reaction mechanism for numerical simulations. In our study, a simplified approach was adopted by prescribing the HRR [22]. The HRR curve for LMO battery boxes was defined based on the numerical results reported by Xie et al. [14]. A mixed-component combustion model was employed to account for the thermal effects of flames, while the concentrations of smoke and gas products were not considered [18]. The total simulation time was set to 200 s, and the ignition temperature of other LIB boxes was set to 120 °C [23,24].

The water mist system had a flow rate of 60.0 L/min per nozzle and a particle velocity of 10 m/s. The investigated droplet sizes ranged from 50 μm to 200 μm, and the spray cone angles ranged from 50° to 80°. A monodisperse droplet assumption was adopted, whereby all injected droplets under the given conditions were assigned the prescribed sizes. The number of computational particles injected was set to 5000 particles/s. A total of 30 water mist nozzles were arranged above the LIB boxes, with each nozzle located 0.15 m above the center of the LIB box. The nozzle activation temperature was set to 65 °C, with a response time index of 50 $(m \cdot s)^{1/2}$. A one-time triggering logic was adopted for nozzle activation. Once activated, the nozzle continued spraying for the remainder of the simulation periods.

It should be noted that direct experimental validation of the predicted thermal propagation behavior and water mist suppression performance was not available for the LIB storage scenarios considered in this study. The quantitative results should be interpreted as model-dependent predictions under the specified LIB storage scenarios and boundary conditions, rather than universally applicable design criteria. Furthermore, once an LIB box was activated, its HRR followed the prescribed time-dependent HRR curve and was not dynamically reduced by water-mist application. Therefore, the temperature reductions discussed above primarily represent the cooling of the surrounding thermal environment and the mitigation of thermal exposure and thermal-runaway propagation, rather than the direct suppression of the internally generated HRR of an already activated LIB box.

2.3. Grid Settings and Sensitivity Analysis

According to the FDS grid calculation formula (Equation (1)), the rational grid size could be ensured to be located between 1/4 and 1/16 of the characteristic flame diameter [25,26], maintaining simulation accuracy. The grid sizes of 0.1 m, 0.12 m, 0.15 m, 0.18 m and 0.2 m were used for grid sensitivity analysis. The HRR curves of five grid sizes under the same fire conditions are shown in Figure 2a. The curves with grid sizes of 0.12 m, 0.15 m and 0.18 m showed similar HRR evolution during the early stages of fire development. However, after 150 s, the results for 0.12 m began to deviate from the two other curves. Furthermore, more pronounced deviations were observed for the 0.1 m and 0.2 m grid curves. Figure 2b showed the temperature variations above the ignition source for different grid sizes. The temperature curves exhibited a rapid rise followed by fluctuations at high temperature levels. For the 0.15 m grid, the temperature curve remained relatively stable compared with other curves. The peak temperatures for 0.1 m, 0.12 m, 0.15 m, 0.18 m and 0.2 m grids were 1232.0 °C, 983.1 °C, 1468.5 °C, 1266.7 °C and 1408.0 °C, respectively. The results indicated that transient temperature variations depended on the grid size, particularly during the intense stage of fire development. Figure 2c showed the temperature variations above the LIB box adjacent to the ignition source under water mist activation

for different grid sizes. For the 0.15 m grid, the water mist system above the adjacent LIB box was activated at 38 s. It provided a relatively stable prediction of the temperature response following water mist activation. The temperature decreased sharply and remained in a relatively stable state without noticeable temperature fluctuations. Considering the computation efficiency and grid analysis results, a grid size of 0.15 m was selected in our study, resulting in a total of 148,135 grid cells. The calculated value of $\frac{D^*}{\delta_x}$ was 12, which lied within the recommended range of 4–16.

$$D^* = \left(\frac{\dot{Q}}{\rho_\infty c_p T_\infty \sqrt{g}} \right)^{\frac{2}{5}}, \quad 4 \le \frac{D^*}{\delta_x} \le 16 \tag{1}$$

where D^* represents the characteristic fire diameter (m); $\dot{Q}$ represents the HRR of the fire source (kW); ρ_∞ is the air density, taken as 1.2 kg/m^3; c_p is the specific heat capacity of air, taken as 1.014 kJ/(kg·K); T_∞ is the ambient temperature, taken as 293 K; g is the gravitational acceleration, taken as 9.8 m/s^2; δ_x represents the grid size (m).

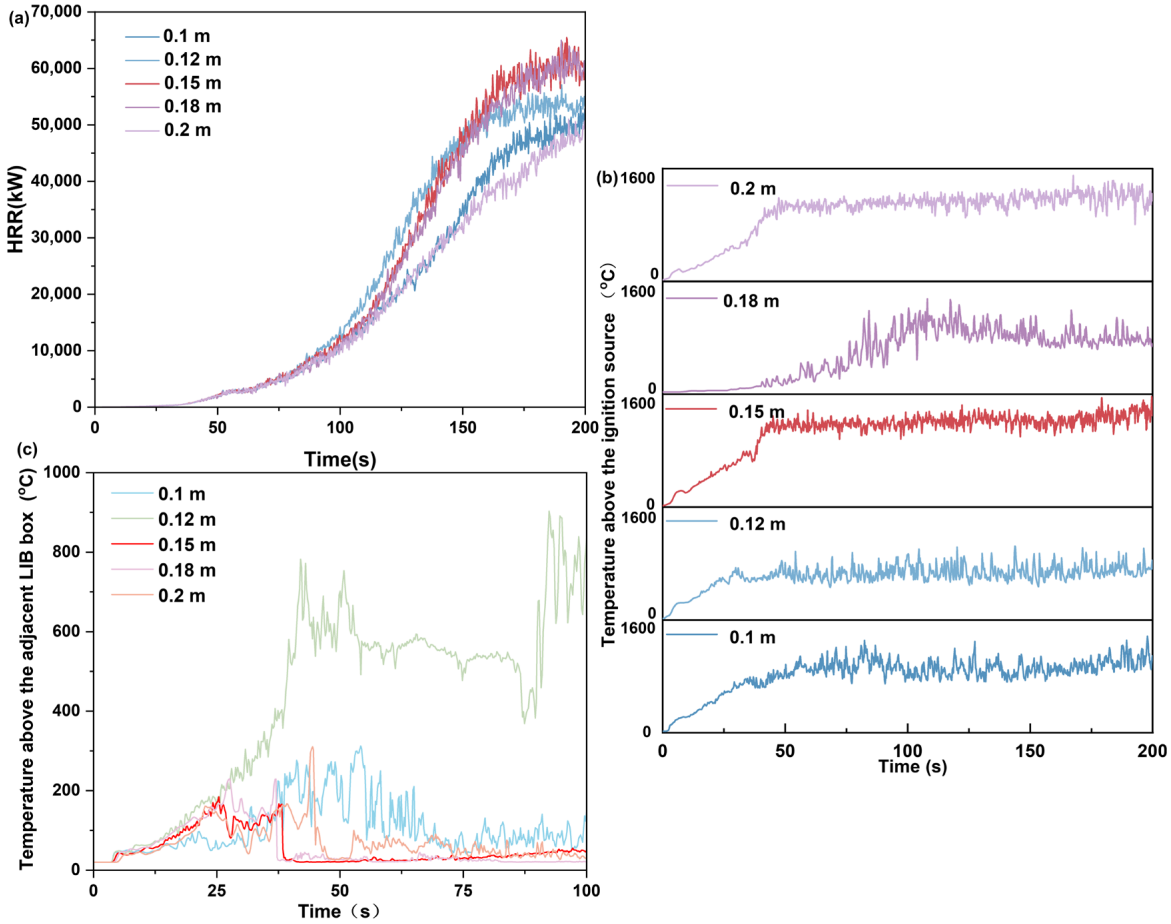


Figure 2. (**a**) HRR comparison; (**b**) temperature variations above the ignition source; (**c**) temperature variations above the LIB box adjacent to the ignition source after water mist activation under different grid sizes.

3. Results and Discussion

3.1. Fire Propagation Characteristics of Different Storage Shelf Types

Three common types of LIB storage shelves, namely a shelf without side baffles, a shelf with side baffles, and a shelf with side baffles and perforated bottom layers, were selected as research objects. Figure 3 shows the temperature distribution slices for different shelf

types at 50 s, 100 s, 150 s, and 200 s after the ignition source battery underwent thermal runaway. The orange and red regions represent high-temperature zones, corresponding to a temperature range of 1200–1500 °C in Figure 3a and 800–1000 °C in Figure 3b,c. For the shelf without side baffles, the flame preferentially propagated in the horizontal direction due to a lack of physical barriers, resulting in a rapid temperature rise in the LIBs at the same shelf. As time progressed, heat propagated upward, gradually affecting the LIBs on the upper shelf levels. With the temperature increasing, thermal radiation became the dominant mode of heat transfer, accelerating the upward fire propagation. By 200 s, all the LIB boxes were engulfed in flames. At this time, the temperatures above the ignition source and at the top of the shelf were measured to be 1216 °C and 973 °C, respectively. In addition, the HRR reached 6.01 $\times$ 10^4 kW. For the shelf with side baffles, the flame preferentially developed in the vertical direction because side barriers inhibited the lateral flame spread. Driven by the unstable jet flame and high temperature toxic gases from the ejected LIB boxes, heat rapidly propagated upward. The temperature of the LIB boxes in the left and right columns increased due to the continued LIB combustion. At 200 s, the HRR reached 2.40 $\times$ 10^4 kW. A total of 18 LIB boxes underwent thermal runaway. For the shelf with side baffles and perforated bottom layers, during 0–100 s, the perforation structure allowed flame and hot gas flow to spread upward unobstructed, resulting in a rapid temperature rise at the top of the shelf. During 100–200 s, heat transferred horizontally along the top of the shelf and affected the LIB boxes stored in the same layer, driven by the ceiling jet effects. At 200 s, the HRR reached 2.09 $\times$ 10^4 kW. Compared with two other shelf conditions, within the 200 s simulation, the shelf with side baffles and perforated bottom layers resulted in the lowest number of LIB boxes affected by thermal runaway at the same time. Therefore, selecting an appropriate shelf type could effectively suppress the flame spread speed and reduce the areas affected by thermal runaway, gaining valuable time for initiating various fire emergency response measures.

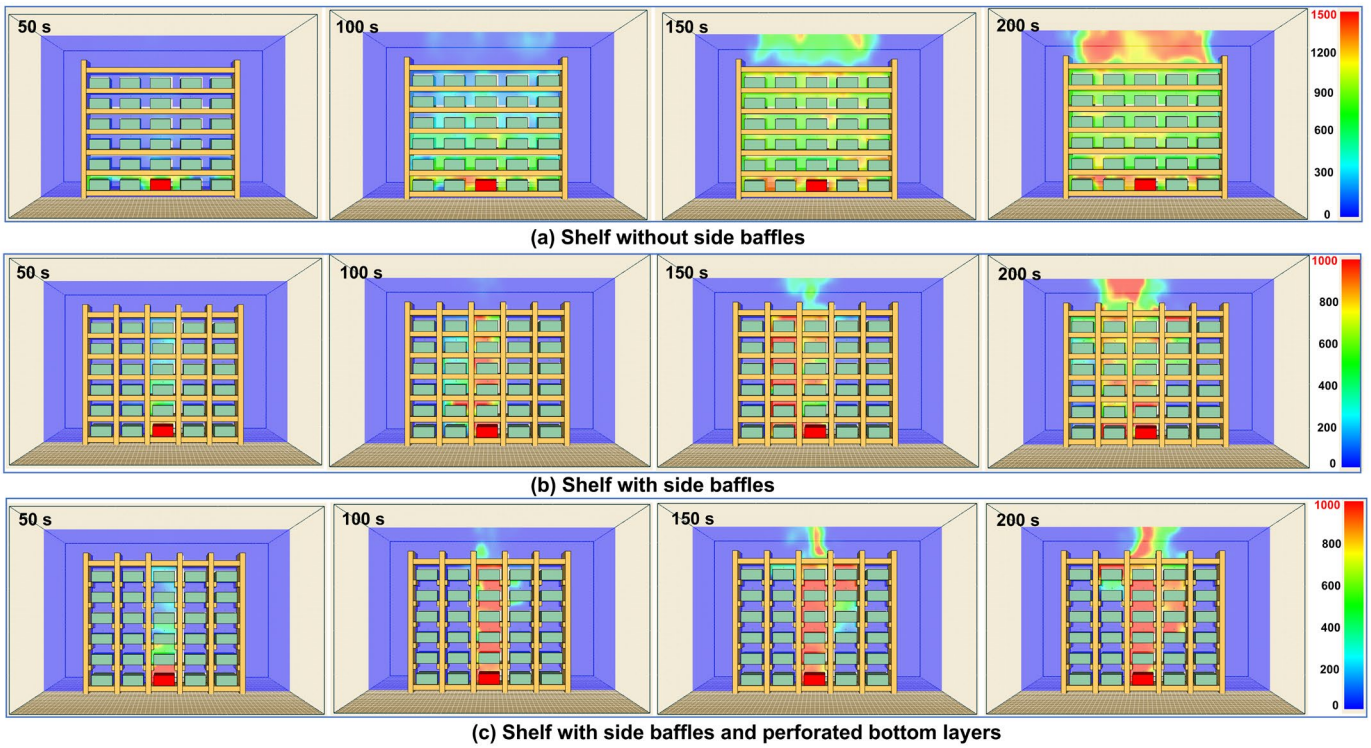


Figure 3. Temperature profile slices of LIB boxes undergoing thermal runaway at different times under: (**a**) the shelf without side baffles; (**b**) the shelf with side baffles; (**c**) the shelf with side baffles and perforated bottom layers.

3.2. Fire Propagation Characteristics of Different LIB Box Horizontal Spacing

An appropriate horizontal spacing could confine heat transfer to a localized propagation pathway and limit thermal propagation to adjacent boxes. Figure 4a exhibited HRR curves of LIB boxes undergoing thermal runaway for horizontal spacings of 0.4 m, 0.6 m, and 0.8 m. The HRRs and average HRR growth rates during 100–200 s are summarized in Table 1. As depicted in Figure 4a, during the initial fire development stage, the HRR curves for the three horizontal spacings were nearly overlapping. However, the HRR curves for horizontal spacings of 0.4 m and 0.6 m maintained a rapid increasing trend, corresponding to the rapid fire development stage with intense heat release. During 100–200 s, the average HRR growth rates for horizontal spacings of 0.4 m and 0.6 m were 97.0 kW/s and 67.2 kW/s, respectively. In contrast, the HRR curve for horizontal spacing of 0.8 m showed three distinct stages, namely a sharp increase, a relatively stable period, and a subsequent decrease. This was consistent with the fire growth stage, the steady combustion stage, and the fire decay stage. During 100–200 s, the average HRR growth rate for the horizontal spacing of 0.8 m was 26.1 kW/s, which was lower than those at the other spacings. Notably, the HRR growth rate dropped to merely 3.6 kW/s during 125–150 s and became negative thereafter. Figure 4b shows the temperature variations measured above the ignited LIB box under different horizontal spacings. During the first 40 s, the temperatures above the ignited LIB box were similar among the three spacings, as the fire was confined to the vicinity of the ignition source and was less affected by the horizontal spacing. After 40 s, the temperatures above the ignited LIB box exhibited a fluctuating upward trend. This can be attributed to the sustained combustion of the LIB box following thermal runaway and the resulting thermal radiation as a dominant mode of heat transfer, proved by the heat flux on the bottom surface of the LIB box above the ignition source (Figure 5). The bottom surface received upward heat transfer from the ignition source. Over the 0–200 s period, the radiative heat transfer accounted for 89.3%, 89.5%, and 89.6% of the total heat transfer. Furthermore, within the same time period, a larger horizontal spacing resulted in a lower temperature above the ignited LIB box. For example, at 115 s, the temperature for horizontal spacings of 0.4 m, 0.6 m and 0.8 m were 936 °C, 825 °C and 686 °C, respectively. The side surface of the LIB box adjacent to the top LIB box was selected as the representative surface. Figure 6 shows the radiative and convective heat fluxes on this surface during the 200 s simulation. During the thermal propagation stage, the radiative heat flux was consistently higher than the convective heat flux. This indicates that radiative heat constituted the dominant heat transfer pathway to the adjacent LIB box. With the spacing increasing from 0.4 m to 0.8 m, the heat flux exhibited a pronounced attenuation trend. For example, the radiative heat flux integrated over 200 s for horizontal spacings of 0.4 m, 0.6 m, and 0.8 m was 585.8 J/m^2, 355.8 J/m^2, and 98.40 J/m^2, respectively. For the horizontal spacing of 0.8 m, the fraction of radiative flux was 99.5% to the total heat release over 200 s. It demonstrated that larger horizontal spacing for mitigating thermal runaway propagation was mainly associated with the reduction in radiative heat transfer among adjacent LIB boxes. These results indicated that increasing the horizontal spacing could effectively reduce the overall heat release intensity and suppress the fire growth rate, thereby mitigating the overall fire severity.

Table 1. HRR (kW) and average HRR growth rates (kW/s) of LIB fires under different horizontal spacings during 100–200 s.

Horizontal Spacing	100 s	125 s	150 s	175 s	200 s	Average HRR Growth Rates
0.4 m	11,243.6	14,767.6	17,840.8	20,197.0	20,939.5	97.0
0.6 m	11,799.9	14,684.5	16,531.4	17,724.3	18,516.5	67.2
0.8 m	10,292.0	13,594.5	13,685.3	13,137.7	12,900.5	26.1

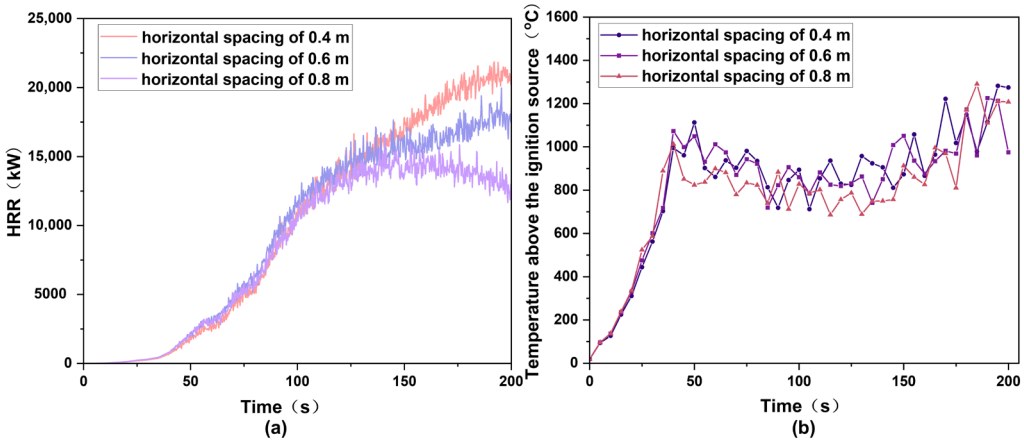


Figure 4. (**a**) HRR curves of LIB boxes undergoing thermal runaway; (**b**) temperature variations above the ignited LIB box for horizontal spacings of 0.4 m, 0.6 m, and 0.8 m.

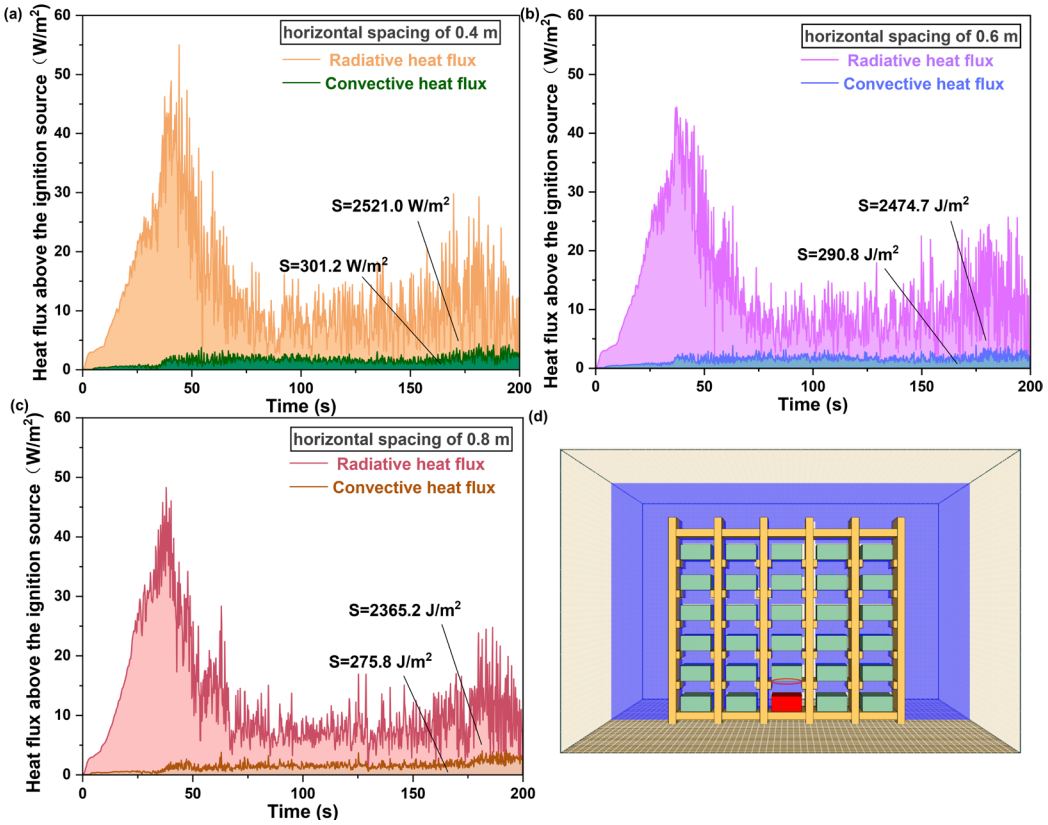


Figure 5. Heat flux on the bottom surface of the LIB box above the ignition source for horizontal spacing of (**a**) 0.4 m, (**b**) 0.6 m, and (**c**) 0.8 m. (**d**) Schematic of the representative surface (circled in red).

3.3. Fire Propagation Characteristics of Different Longitudinal Shelf Spacing

In actual LIB storage scenarios, shelves were arranged in multiple rows along the longitudinal direction. A reasonable longitudinal shelf spacing could directly determine the time available for flames to propagate to adjacent shelves following thermal runaway. Figure 7 exhibits the temperature variations at the top of the adjacent shelf (designated as shelf 2) at longitudinal spacings of 0.8 m, 1.2 m, and 1.5 m. At the longitudinal spacing of 0.8 m, the temperature at the top of shelf 2 increased sharply and reached the peak at 100 s. In contrast, the onsets of the rapid temperature rise were significantly delayed at the longitudinal spacings of 1.2 m and 1.5 m. In the numerical simulations, the ignition temperature of the LIB box was set to 120 °C. For the longitudinal spacings of 0.8 m, 1.2 m, and 1.5 m,

the temperatures at the top of shelf 2 exceeded 120 °C at 43 s, 75 s, and 87 s, respectively. To evaluate the influence of the triggering temperature, the sensitivity analysis was performed by increasing the triggering temperature of 140 °C and 160 °C, as summarized in Table 2. The propagation times to adjacent shelves at triggering temperatures of 140 °C and 160 °C were 45 s and 47 s for the shelf spacing of 0.8 m; 78 s and 81 s for the shelf spacing of 1.2 m; and 90 s and 94 s for 1.5 m, respectively. The small variation in propagation time was associated with the rapid temperature rise immediately preceding the prescribed thermal runaway activation. For longitudinal shelf spacings of 0.8 m, 1.2 m, and 1.5 m, the rapid temperature rise began at approximately 40 s, 70 s, and 85 s, respectively, with the average temperature rise rates of 18.6 °C/s, 13.8 °C/s, and 9.8 °C/s over the subsequent 5 s. Once the LIB box entered the rapid heating stage, the additional time required to reach a higher triggering temperature was relatively short. More importantly, the effects of longitudinal shelf spacing on thermal runaway propagation remained consistent across all three triggering temperatures. Figure 8 showed the fire spreading behavior at a longitudinal spacing of 1.5 m at 90 s. Fire was observed on shelf 2 at 90 s, which further illustrated the predicted fire propagation process. Thus, arranging the larger longitudinal shelf spacing could delay the ignition of LIB boxes on the adjacent shelf and mitigate the associated fire losses.

Table 2. The sensitivity analysis of the thermal runaway triggering temperature of the LIB box.

Longitudinal Spacing	120 °C	140 °C	160 °C	Average Temperature Rise Rates
0.8 m	43 s	45 s	47 s	18.6 °C/s (40–45 s)
1.2 m	75 s	78 s	81 s	13.8 °C/s (70–75 s)
1.5 m	87 s	90 s	94 s	9.8 °C/s (85–90 s)

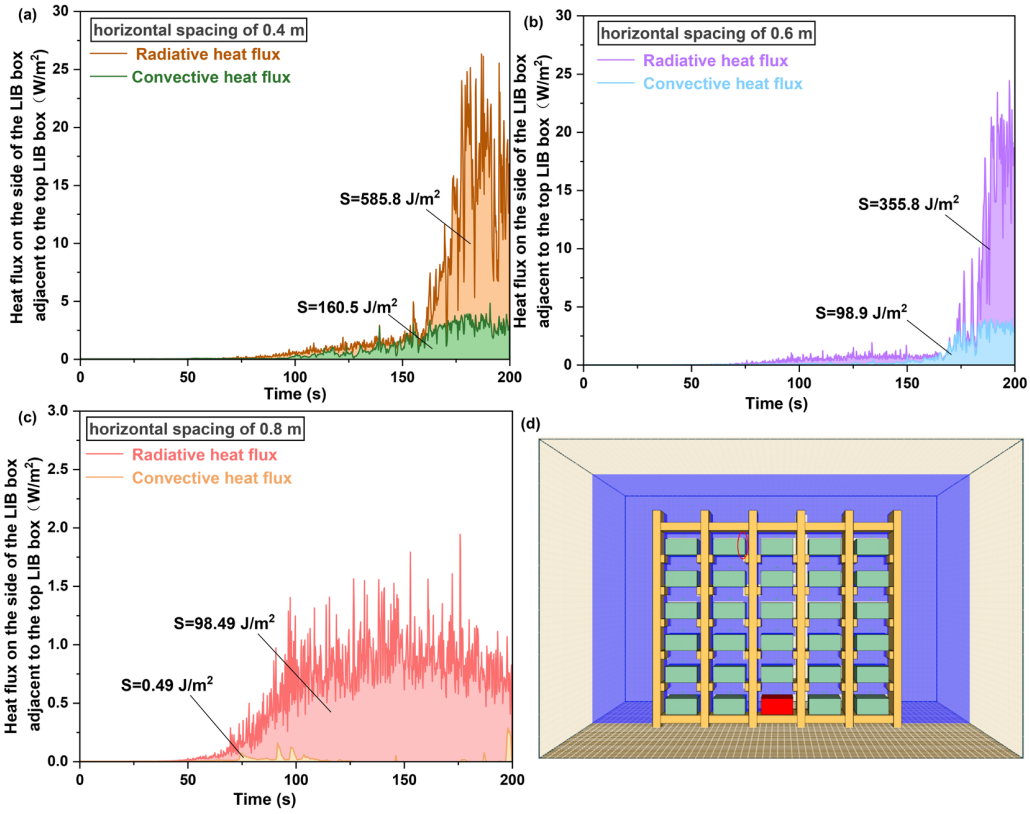


Figure 6. Heat flux on the side surface of the LIB box adjacent to the top LIB box for horizontal spacing of (**a**) 0.4 m, (**b**) 0.6 m, and (**c**) 0.8 m. (**d**) Schematic of the representative surface (circled in red).

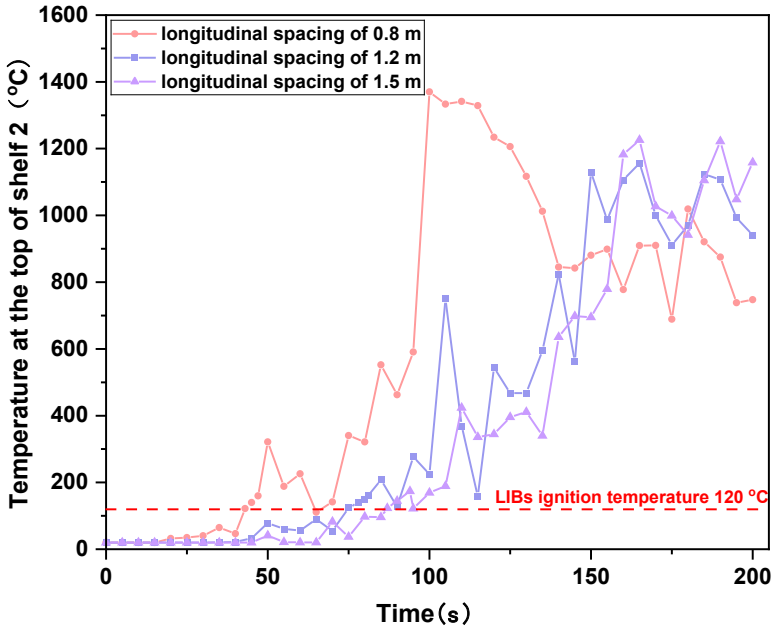


Figure 7. Temperature variation curves at the top of the adjacent shelf (designated as shelf 2) following thermal runaway at longitudinal shelf spacings of 0.8 m, 1.2 m, and 1.5 m.

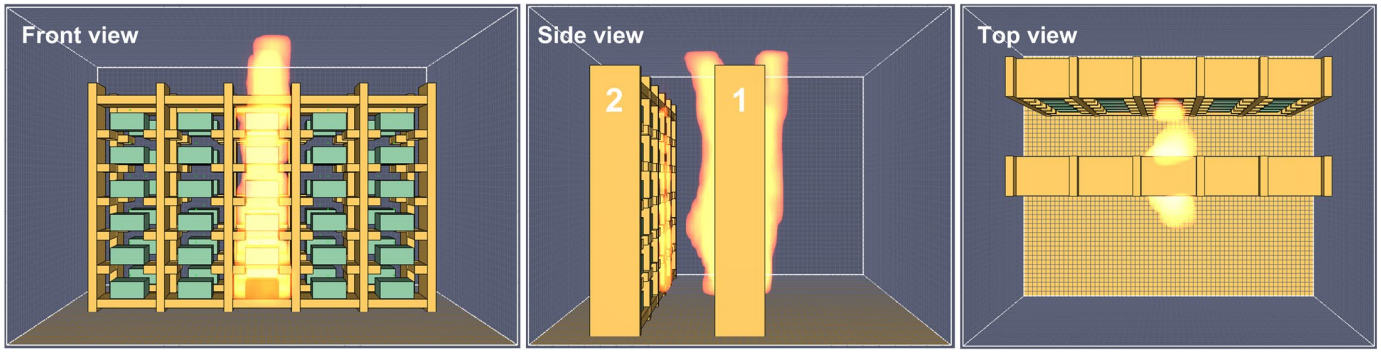


Figure 8. Fire spreading behavior at a longitudinal shelf spacing of 1.5 m at 90 s, viewed from different angles. (Note: The shelf of fire origin was labeled 1, and the adjacent shelf was labeled 2).

3.4. Suppression Performance of Water Mist System for LIB Fires

3.4.1. Droplet Size Sensitivity of Water Mist

According to the American NFPA 750 standard [27], water mist is defined as a spray with a droplet size at 99% cumulative volume ($D_{v0.99}$) of less than 1000 μm. Specifically, Level I water mist is specified by droplet sizes of ≤100 μm for ($D_{v0.1}$) and ≤200 μm for ($D_{v0.9}$). It exhibited excellent substantial cooling and thermal mitigation during fire exposure due to the high degree of atomization [28,29]. As shown in Figure 9, droplet sizes of 50 μm, 100 μm, 150 μm, and 200 μm were investigated to evaluate their fire suppression effects. Figure 9a,b showed the temperature variation curves above the ignition source and at the top of the shelf, respectively. Driven by thermal runaway of the ignited LIB box, the temperature above the ignition source increased sharply and reached a peak value of 417 °C. When the temperature reached the activation threshold of the water mist nozzle, the water mist system equipped above the ignition source was activated at 23 s, resulting in a rapid decrease in temperature. For a droplet with 50 μm, the temperature decreased most significantly, dropping rapidly from 417 °C to below 100 °C and stabilizing at 100 °C with minimal fluctuations. Figure 9c presents the temperature distributions on the shelf at different times for a droplet size of 50 μm, further demonstrating its superior cooling

effect. In contrast, larger droplets resulted in a transient temperature decrease, followed by substantial rebounds and high temperature oscillations. For example, for a droplet size of 200 μm, the temperature briefly dropped and rebounded to 390 °C within 10 s, remaining at 267 °C on average within the subsequent 20 s. Furthermore, owing to the unstable jet flames and the fire plume, the thermal impact subsequently extended up the shelf, leading to a temperature increase at the top of the shelf. For a droplet size of 50 μm, the water mist spray system at the top of the shelf was activated at 56 s, which was later than for other larger droplet sizes. The delayed activation suggested that, among the investigated droplet sizes, arranging a 50 μm water mist system could effectively cool the ambient temperature, inhibit heat transfer, and mitigate the thermal impact on the upper LIB boxes during the initial fire stage. Compared with larger droplets, smaller droplets could have a positive effect on enhancing thermal mitigation performance. This could be attributed to a larger specific surface area and the rapid evaporation process upon contact with the flame for smaller droplets. The evaporation process could absorb a large amount of heat and generate substantial water vapor, consequently reducing the temperature near the flame zone. Meanwhile, the larger specific surface area could promote heat transfer and accelerate water evaporation rates, enhancing the fire suppression effects [30,31]. However, although the water mist exerted a positive effect in cooling and thermal mitigation, the internal thermal runaway reactions in the activated LIB box were not terminated during the 200 s simulation.

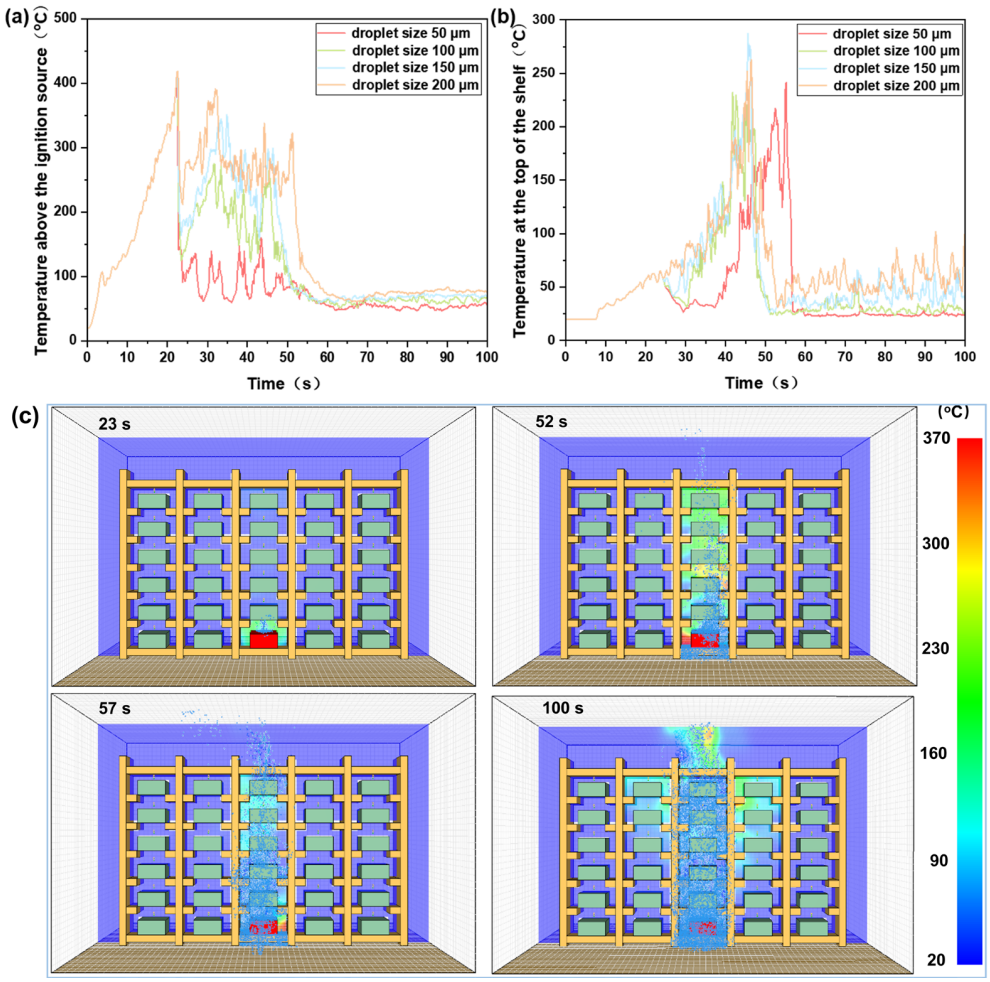


Figure 9. Temperature variation curves (**a**) above the ignition source; (**b**) at the top of the shelf under water mist droplet sizes of 50 μm, 100 μm, 150 μm, and 200 μm; (**c**) temperature distribution slices on the shelf at 23 s, 52 s, 57 s, and 100 s when the water mist droplet size was 50 μm.

3.4.2. Spray Cone Angles of Water Mist

An appropriate spray cone angle determines the spatial distribution of water mist and the effective coverage area within the fire zone, which is one of the most significant factors in improving fire suppression performance. As depicted in Figure 10a, when the water mist nozzle was positioned 0.15 m above the LIB box, the minimum coverage angle covering one LIB box was calculated to be 75°. Accordingly, we investigated the influence of spray cone angle on fire suppression performance by setting the angles to 50°, 65°, 75°, and 80°, as shown in Figure 10b. As the spray cone angle decreased, the temperature above the ignition source exhibited more pronounced fluctuations and stronger rebound peaks, due to insufficient spray coverage. For instance, at a spray cone angle of 50°, four rebound peaks exceeding 300 °C were observed within 20 s of water mist activation, indicating unstable fire suppression. In contrast, at a spray cone angle of 75°, the temperature above the ignition source rapidly decreased from 417 °C to 98 °C and fluctuated around 100 °C within 40 s of water mist activation, eventually dropping to below 50 °C. The enhanced cooling performance at a 75 ° angle could be attributed to sufficient coverage of all of the burning LIBs, which facilitated sustained contact between droplets and flame. However, when increasing the angle to 80°, a negligible improvement in cooling performance was observed, showing the margin effect. Therefore, a spray cone angle of 75° served as the most favorable spray cone angle investigated for the LIB box shelf storage.

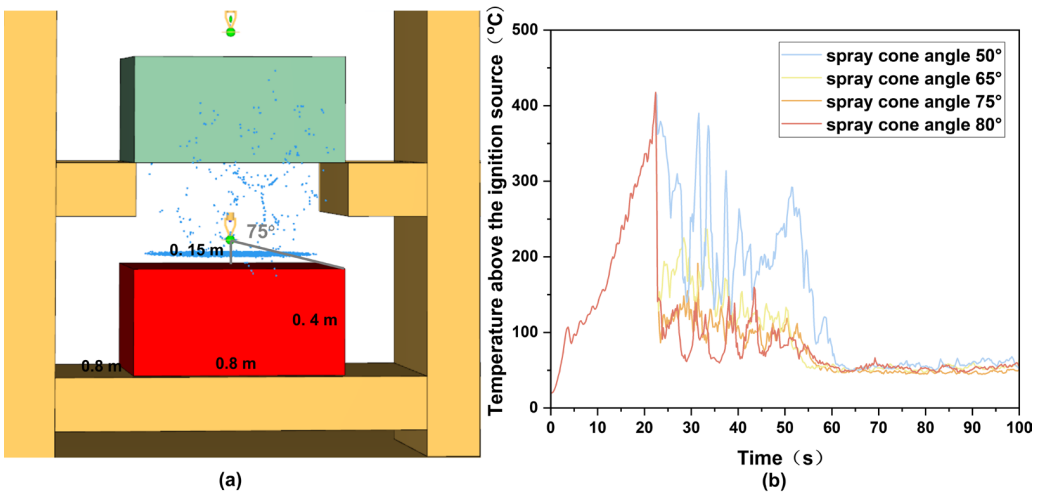


Figure 10. (**a**) Schematic diagram of the water mist spray system installed above the LIB box; (**b**) temperature variation curves above the ignition source at spray cone angles of 50°, 65°, 75°, and 80°.

4. Conclusions

In this paper, numerical simulations of thermal runaway in LMO LIB boxes were carried out based on actual shelf storage scenarios to investigate the fire behavior of LIB boxes stored on shelves and the fire suppression performance of water mist systems. Under the investigated conditions and periods, the conclusions were as follows:

(1) Among the shelf types investigated, the shelf with side baffles and perforated bottom layers was identified as the most effective type for limiting the extent of fire propagation, resulting in the lowest number of LIB boxes undergoing thermal runaway within 200 s.

(2) Increasing the horizontal spacing between LIB boxes to 0.8 m reduced the radiant heat transfer from adjacent burning LIB boxes, yielding the lowest average HRR growth rate of 26.1 kW/s during 100–200 s.

(3) Increasing the longitudinal shelf spacing to 1.5 m reduced the fire propagation tendency to neighboring shelves and delayed the ignition of LIB boxes on the top of the neighboring shelves to 87 s at the triggering temperature of 120 °C.
(4) For LIB fires, the water mist system exhibited the most favorable fire suppression, especially in terms of cooling and thermal mitigation at a droplet size of 50 μm and a spray cone angle of 75° among the investigated parameters.

For large-scale LIB storage, our numerical study elucidates the effects of shelf configurations, storage layouts, and water mist system parameters on fire propagation and suppression strategies, providing a basis for understanding the relative effects of these parameters and a numerical reference for further experimental investigations and fire protection design studies. Further work will investigate the fire characteristics of LIBs with varying SOC and battery types under water mist suppression and conduct dedicated validation experiments to better reflect realistic LIB storage conditions.

Author Contributions: Conceptualization, Q.Z. and B.Z.; methodology, Q.Z.; software, H.Z. and W.H.; validation, Q.Z. and Z.Z.; formal analysis, Z.Z. and H.Z.; data curation, L.Y. and W.H.; writing—original draft preparation, Q.Z.; writing—review and editing, L.Y. and B.Z.; supervision, B.Z.; project administration, H.Z.; funding acquisition, Q.Z. and B.Z. All authors have read and agreed to the published version of the manuscript.

Funding: This research was funded by the Chengdu Science and Technology Program, grant number 2025-YF09-00062-SN; Research Project of China Fire and Rescue Institute, grant number YY202606-08; Special Project for Research and Development in Key Areas of Guangdong Province, grant number 2024B1111080003.

Data Availability Statement: The original contributions presented in this study are included in the article.

Conflicts of Interest: The authors declare no conflicts of interest.

References

1. Khan, F.M.N.U.; Rasul, M.G.; Sayem, A.S.M.; Mandal, N.K. Design and optimization of lithium-ion battery as an efficient energy storage device for electric vehicles: A comprehensive review. *J. Energy Storage* **2023**, *71*, 108033. [CrossRef]
2. Wang, Q.; Mao, B.; Stoliarov, S.I.; Sun, J. A review of lithium ion battery failure mechanisms and fire prevention strategies. *Prog. Energy Combust. Sci.* **2019**, *73*, 95–131. [CrossRef]
3. Kumar, R.; Das, K. Lithium battery prognostics and health management for electric vehicle application—A perspective review. *Sustain. Energy Technol. Assess.* **2024**, *65*, 103766. [CrossRef]
4. Jeevarajan, J.A.; Joshi, T.; Parhizi, M.; Rauhala, T.; Juarez-Robles, D. Battery hazards for large energy storage systems. *ACS Energy Lett.* **2022**, *7*, 2725–2733. [CrossRef]
5. Cui, Y.; Shen, X.; Zhang, H.; Yin, Y.; Yu, Z.; Shi, D.; Fang, Y.; Xu, R. Intrinsic safety risk control and early warning methods for lithium-ion power batteries. *Batteries* **2024**, *10*, 62. [CrossRef]
6. Lai, X.; Jin, C.; Yi, W.; Han, X.; Feng, X.; Zheng, Y.; Ouyang, M. Mechanism, modeling, detection, and prevention of the internal short circuit in lithium-ion batteries: Recent advances and perspectives. *Energy Storage Mater.* **2021**, *35*, 470–499. [CrossRef]
7. Mao, Y.; Chen, Y.; Chen, M. Review of flame behavior and its suppression during thermal runaway in lithium-ion batteries. *Batteries* **2024**, *10*, 307. [CrossRef]
8. Qi, L.; Wang, Y.; Kong, L.; Yi, M.; Song, J.; Hao, D.; Zhou, X.; Zhang, Z.; Yan, J. Manufacturing processes and recycling technology of automotive lithium-ion battery: A review. *J. Energy Storage* **2023**, *67*, 107533. [CrossRef]
9. Jia, Z.; Jin, K.; Mei, W.; Qin, P.; Sun, J.; Wang, Q. Advances and perspectives in fire safety of lithium-ion battery energy storage systems. *eTransportation* **2025**, *24*, 100390. [CrossRef]
10. Zhang, L.; Jin, K.; Sun, J.; Wang, Q. A review of fire-extinguishing agents and fire suppression strategies for lithium-ion batteries fire. *Fire Technol.* **2024**, *60*, 817–858. [CrossRef]
11. *GB 50016-2014*; Code for Fire Protection Design of Buildings (2018 Edition). China Planning Press: Beijing, China, 2018.
12. *DB4403/T 508-2024*; Safety Specification for Storing and Using of Lithium-Ion Batteries in Production and Business Unit. Shenzhen Municipal Administration for Market Regulation: Shenzhen, China, 2024.

13. Wang, Z.; Sadeghi, H.; Huang, X.; Restuccia, F. Thermal runaway and flame propagation in battery packs: Numerical simulation and deep learning prediction. *Eng. Appl. Comput. Fluid Mech.* **2025**, *19*, 2445160. [CrossRef]
14. Xie, J.; Li, J.; Wang, J.; Jiang, J. Fire protection design of a lithium-ion battery warehouse based on numerical simulation results. *J. Loss Prev. Process Ind.* **2022**, *80*, 104885. [CrossRef]
15. Cui, Y.; Chen, Y.; Chen, M.; Ouyang, D.; Weng, J.; Tao, C.; Zhao, L.; Wang, J. Numerical study on the fire and its propagation of large capacity lithium-ion batteries under storage. *J. Therm. Anal. Calorim.* **2023**, *148*, 5787–5803. [CrossRef]
16. Mishra, D.; Tummala, R.; Jain, A. Investigation of propagation of thermal runaway during large-scale storage and transportation of Li-ion batteries. *J. Energy Storage* **2023**, *72*, 108315. [CrossRef]
17. Wang, Z.; Song, Y.; Yin, B.; Shi, B.; Li, Z.; Yu, J. Effect of ambient pressure on the fire characteristics of lithium-ion battery energy storage container. *J. Loss Prev. Process Ind.* **2024**, *92*, 105459. [CrossRef]
18. Lou, Z.; Huang, J.; Wang, M.; Zhang, Y.; Lv, K.; Yao, H. Inhibition performances of lithium-ion battery pack fires by fine water mist in an energy-storage cabin: A simulation study. *Phys. Fluids* **2024**, *36*, 045141. [CrossRef]
19. McGrattan, K.; Hostikka, S.; McDermott, R.; Floyd, J.; Weinschenk, C.; Overholt, K. *Fire Dynamics Simulator Technical Reference Guide Volume 1: Mathematical Model*; National Institute of Standards and Technology: Gaithersburg, MD, USA, 2013; pp. 13–21.
20. McGrattan, K.B.; Baum, H.R.; Rehm, R.G. Large eddy simulations of smoke movement. *Fire Saf. J.* **1998**, *30*, 161–178. [CrossRef]
21. McGrattan, K.; McDermott, R.; Floyd, J.; Hostikka, S.; Forney, G.; Baum, H. Computational fluid dynamics modelling of fire. *Int. J. Comput. Fluid Dyn.* **2012**, *26*, 349–361. [CrossRef]
22. Brzezinska, D.; Bryant, P. Performance-based analysis in evaluation of safety in car parks under electric vehicle fire conditions. *Energies* **2022**, *15*, 649. [CrossRef]
23. Yuan, W.; Liang, D.; Chu, Y.; Wang, Q. Aging effect delays overcharge-induced thermal runaway of lithium-ion batteries. *J. Loss Prev. Process Ind.* **2022**, *79*, 104830. [CrossRef]
24. Lei, B.; Zhao, W.; Ziebert, C.; Uhlmann, N.; Rohde, M.; Seifert, H.J. Experimental analysis of thermal runaway in 18650 cylindrical Li-ion cells using an accelerating rate calorimeter. *Batteries* **2017**, *3*, 14. [CrossRef]
25. Sellami, I.; Manescau, B.; Chetehouna, K.; Izarra, C.d.; Nait-Said, R.; Zidani, F. BLEVE fireball modeling using Fire Dynamics Simulator (FDS) in an Algerian gas industry. *J. Loss Prev. Process Ind.* **2018**, *54*, 69–84. [CrossRef]
26. McDermott, R.J.; Forney, G.P.; McGrattan, K.; Mell, W.E. Fire dynamics simulator version 6: Complex geometry, embedded meshes, and quality assessment. In Proceedings of the V European Conference on Computational Fluid Dynamics (ECCOMAS CFD 2010), Lisbon, Portugal, 14–17 June 2010.
27. *National Fire Protection Association (NFPA) 750*; Standard on Water Mist Fire Protection Systems. National Fire Protection Association (NFPA): Quincy, MA, USA, 2023.
28. Mawhinney, J.R.; Dlugogorski, B.Z.; Kim, A.K. A closer look at the fire extinguishing properties of water mist. In Proceedings of the Fourth International Symposium on Fire Safety Science, Ottawa, ON, Canada, 13–17 June 1994.
29. Ji, C.; Liu, Y.; Qi, P.; Zhang, Z.; Zhang, S. Simulation investigation of water spray on suppressing lithium-ion battery fires. *Fire Technol.* **2023**, *59*, 1221–1246. [CrossRef]
30. Ferng, Y.; Liu, C. Numerically investigating fire suppression mechanisms for the water mist with various droplet sizes through FDS code. *Nucl. Eng. Des.* **2011**, *241*, 3142–3148. [CrossRef]
31. Liu, J.; He, M. Modeling and analysis of key factors influencing water mist fire suppression efficiency. *Processes* **2026**, *14*, 205. [CrossRef]

Disclaimer/Publisher's Note: The statements, opinions and data contained in all publications are solely those of the individual author(s) and contributor(s) and not of MDPI and/or the editor(s). MDPI and/or the editor(s) disclaim responsibility for any injury to people or property resulting from any ideas, methods, instructions or products referred to in the content.